Journal of Alloys and Compounds, 194 (1993) 381–387
JALCOM 7203

Electron-irradiation-induced crystalline-to-amorphous transition in transition metal borides

H. Mori and T. Sakata
Research Centre for Ultra-High Voltage Electron Microscopy, Osaka University, Yamadaoka, Suita, Osaka 565 (Japan)

(Received April 22, 1992; in final form May 12, 1992)

Abstract

A series of transition metal borides were irradiated with 2 MeV electrons in a high voltage electron microscope, and the presence (or absence) of the crystalline–amorphous (C–A) transition was examined. In total, 14 compounds were investigated and it was revealed that such a C–A transition was induced in eight of the compounds. Analysis of the results shows that the tendency toward the C–A transition under electron irradiation is best correlated with the position of the compounds in the corresponding *T–C* phase diagram.

1. Introduction

In 1982 it was discovered that high energy (MeV) electron irradiation can induce a crystalline to amorphous (C–A) transition in some intermetallic compounds such as NiTi [1, 2] and Fe_3B [3]. Occurrence of an incomplete C–A transition in Zr_3Al was reported by Carpenter and Schulson [4] in 1978. Their results suggested that the C–A transition occurred only in regions close to lattice defects and not in the crystalline matrix. Recently it has been suggested that a C–A transition in Zr_3Al under electron irradiation is induced only when impurity atoms such as hydrogen and oxygen are to some extent included in the crystal lattice [5].

Therefore there is a possibility that the incomplete C–A transition in Zr_3Al observed by Carpenter and Schulson is not an intrinsic transition. For this reason the compound Zr_3Al is not listed here.

This C–A transition is caused not by ionization damage but by displacement damage [1, 2]. It is of interest because of the simplicity of electron irradiation damage. The simplicity firstly comes from the fact that the energy transferred to the primary knock-on atoms from a few mega electronvolts of incident electrons is sufficient to produce only single or at most double atom displacements. This is in sharp contrast to the massive damage in the form of a displacement cascade produced by ion and neutron irradiation, where a complex process analogous to liquid phase quenching or vapour phase quenching might be operative in the damage core region. Secondly, the chemical composition of target materials remains constant during the electron irradiation since impurity atoms are neither introduced nor created in the materials, which is not the case with ion and neutron irradiation. Such simplicity in experimental conditions makes the C–A transition a good candidate for an investigation of the solid-state amorphization. Based upon this premise a systematic study has been made of the electron-irradiation induced C–A transition in intermetallics by a research group at Osaka University [6, 7], with the use of a 2 MV high voltage electron microscope (HVEM); a series of intermetallic compounds in aluminium–transition metal (Al–T) systems [7] and in transition metal–transition metal (T–T) systems [6] have so far been irradiated with 2 MeV electrons and the presence (or absence) of the C–A transition has been examined. It is revealed that the amorphization tendency of these intermetallic compounds is best correlated with the position of the compounds in the phase diagram [7]. Those compounds whose position in the diagram is close to the bottom of a deep valley of the liquidus have a strong tendency towards the C–A transition.

As an extension of the above work, the amorphization tendency of transition metal borides was examined in the present study. A total of 14 compounds were investigated and it was revealed that a C–A transition was induced in eight of them. Analysis of the results shows that there again exists a close linkage between the amorphization tendency under electron irradiation and the position of the compounds in the phase diagram.

2. Specimens and experimental procedures

The 14 materials examined in this work are listed in the first column of Table 1. Details of specimen

0925-8388/93/$6.00

TABLE 1. Crystal stability under 2 MeV electron irradiation of transition metal borides

Compound	Response	Crystal system	Crystal structure	n/unit cell	Extent of solubility (at.%)
Mn_4B	○	Orthorhombic	D_{2h}^{24}	48	None
Mn_2B	×	Tetragonal	C16	12	None
Fe_3B	○	Orthorhombic	D_{2h}^{16}	16	None
Fe_2B	○	Tetragonal	C16	12	None
Ta_2B	○	Tetragonal	C16	12	None
TaB_2	×	Hexagonal	C32	3	8
Co_3B	○	Orthorhombic	D_{2h}^{16}	16	None
Co_2B	○	Tetragonal	C16	12	None
CoB	×	Orthorhombic	B27	8	None
Ni_3B	×	Orthorhombic	DO_{11}	16	None
Ni_2B	○	Tetragonal	C16	12	None
o-Ni_4B_3	○	Orthorhombic	D_{2h}^{16}	28	None
m-Ni_4B_3	×	Monoclinic	C_{2h}^{6}	28	None
NiB	×	Orthorhombic	Bf	8	None

preparation are given elsewhere [8, 9]. All the specimens were irradiated with 2 MeV electrons in the 2 MV HVEM, and changes in the bright-field images as well as in the selected area diffraction patterns (SADs) were monitored *in situ* during the irradiation. The criterion used to define the occurrence of the C–A transition was the complete replacement of crystalline spot patterns by diffuse ring patterns in the SADs. Electron irradiation of compounds in the nickel–boron system was carried out at approximately 4 K. All other compounds were irradiated at about 100 K. The electron flux was fixed at around 1×10^{24} e m^{-2} s^{-1} throughout the experiment.

3. Results

Of the 14 compounds investigated here, eight compounds such as Mn_4B, Fe_3B, Fe_2B, Ta_2B, Co_3B, Co_2B, Ni_2B and o-Ni_4B_3 underwent a C–A transition under irradiation, while the other six remained crystalline. This indicates that the C–A transition is also a general phenomenon in transition metal borides. The presence (or absence) of the C–A transition in individual compounds is given in the second column in Table 1, where the symbols ○ and × denote the presence and absence of the C–A transition respectively.

3.1. Transition metal borides that can be rendered amorphous

An example of the C–A transition is shown in Fig. 1, where successive stages of the C–A transition in Mn_4B are illustrated in sequence. Here the incident beam is parallel to the $[1\bar{1}\bar{3}]$ direction. The irradiation temperature was 100 K. Figures 1(a)–(c) show bright-field images before irradiation, after irradiation for 0.6 ks and 1.8 ks respectively. The arrows indicate a fixed position. The corresponding SADs are illustrated in Figs. 1(a')–(c'). Before irradiation, well-defined bend contours are observed in the image (Fig. 1(a)) and the $[1\bar{1}\bar{3}]$ net pattern is apparent in the SAD (Fig. 1(a')). In the early stages of irradiation a high density of secondary defects is produced in the irradiated area (Fig. 1(b)). In the corresponding SAD diffuse rings appear superimposed on the net pattern (Fig. 1(b')), indicating the occurrence of local amorphization. Finally, all the Bragg diffraction contrasts disappear and an area of uniform contrast is produced at the central portion of the irradiated area (encircled by a dotted line in Fig. 1(c)), and at this stage the corresponding SAD changes from the original spot pattern (Fig. 1(a')) to a halo pattern (Fig. 1(c')), showing the completion of the amorphization. This amorphization process is essentially the same as that observed in T–T and Al–T intermetallic compounds [6]. All other seven compounds were rendered amorphous via a similar process [8, 9].

It is reported by Mogro-Campero *et al.* [3] that Fe_3B can be rendered amorphous by 1 MeV electron irradiation at 130 K whereas Fe_2B is not affected by the irradiation. In the present work it is shown that both Fe_3B and Fe_2B become amorphous under 2 MeV electron irradiation at 100 K. The damage rate for the condition of the present experiment is estimated to be 8×10^{-3} dpa s^{-1} if a value of 24 eV is used for the displacement energy of iron and no corrections for boron are taken into account. This rate is approximately seven times as high as that employed in the experiment by Mogro-Campero *et al.* [3]. The high damage rate as well as the low irradiation temperature used in the present work seem to favour the C–A transition in Fe_2B.

3.2. Transition metal borides that remains crystalline

In Fig. 2 is depicted an example of the behaviour of transition metal borides that remain crystalline under irradiation. Figure 2(a) shows an area of a foil of Mn_2B before irradiation and the corresponding SAD is illustrated in Fig. 2(a'). The arrows indicate a fixed position. Figures 2(b) and 2(c) show the same area after irradiation for 360 s and 3.6 ks respectively. As seen from these figures, the irradiation certainly induces the formation of secondary defects; but even after irradiation for 3.6 ks signs of a C–A transition were recognized neither in the bright-field image nor in the SAD. Such behaviour is characteristic of transition metal borides that remain crystalline.

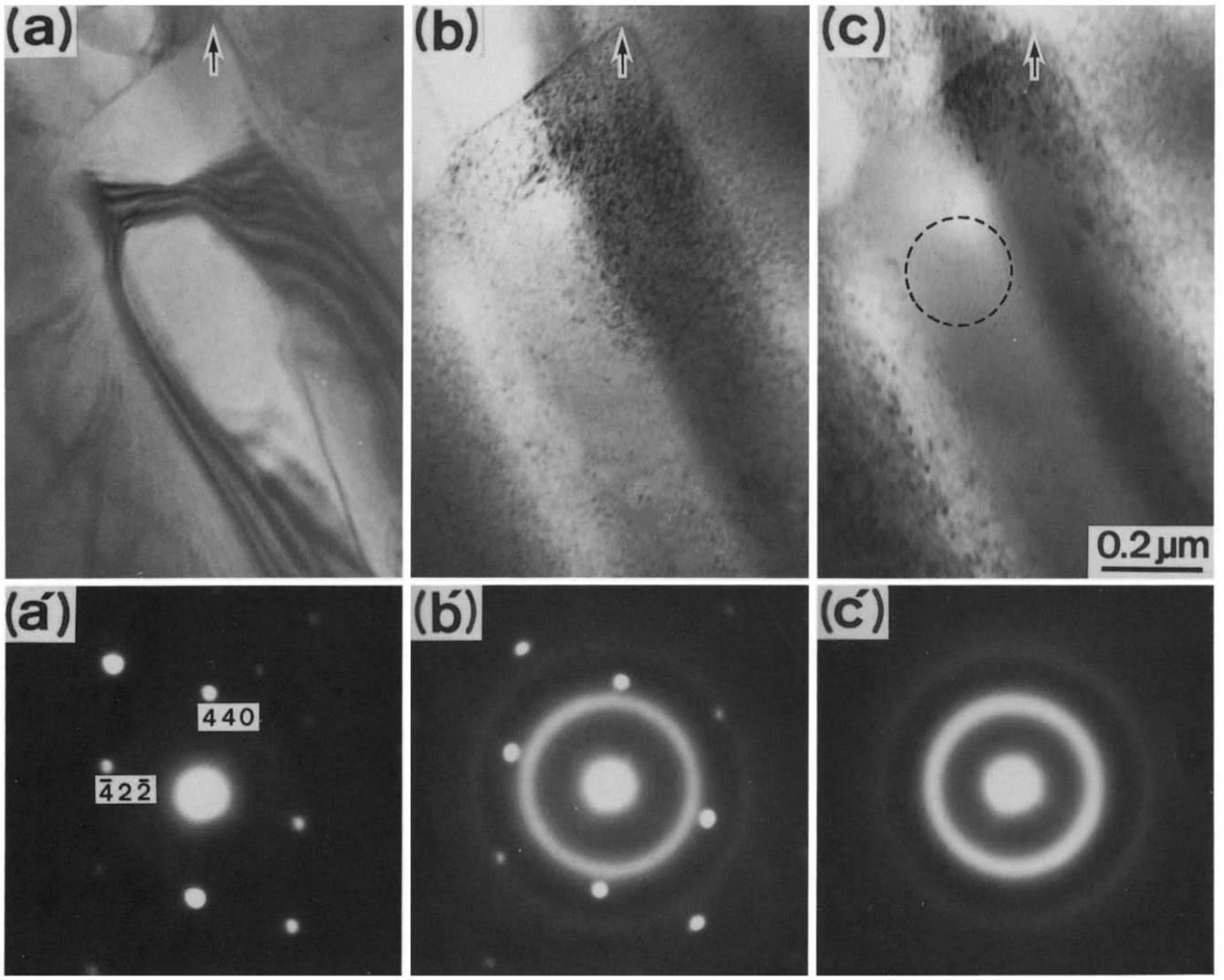

Fig. 1. Successive stages of the amorphization of Mn_4B by 2 MeV electron irradiation with corresponding diffraction patterns. The arrows mark a fixed position. Irradiation temperature and flux were approximately 100 K and 1×10^{24} e m^{-2} s^{-1} respectively. (a) Before irradiation; (b) after 0.6 ks irradiation; (c) after 1.8 ks irradiation (the circle depicts the central portion of the irradiated area).

4. Discussion

On the basis of the results summarized in Table 1, the factors affecting the amorphization tendency will now be discussed. The third column of Table 1 lists the crystal system of each material. It is, however, impossible to make a consistent arrangement of the amorphization tendency based on this parameter of the crystal system, since some (*e.g.* Mn_4B, Fe_3B and Co_3B) of the transition metal borides of the orthorhombic system become amorphous, while others (*e.g.* CoB, Ni_3B and NiB) do not. The parameter of crystal system is thus thought not to be a critical factor.

The fourth and fifth columns of Table 1 list crystal structure (or space group) and the number of atoms in a unit cell respectively. These two parameters are both related to the complexity of the crystal structure. It has been suggested that intermetallic compounds with complex crystal structures have a high possibility of becoming amorphous under electron irradiation [10]. It is, however, again difficult to make a systematic arrangement of the observed amorphous-forming ability in terms of these two parameters. For example, some (*e.g.* Fe_2B, Ta_2B, Co_2B and Ni_2B) of the transition metal borides with the C16 structure ($n=12$) can be rendered amorphous while others (*e.g.* Mn_2B) cannot. The complexity of the crystal structure therefore seems not to be an essential factor.

The sixth column of Table 1 lists the composition phase field of each material in the corresponding phase diagram. This parameter is listed to check whether the solubility criterion by Brimhall *et al.* [11] is valid or

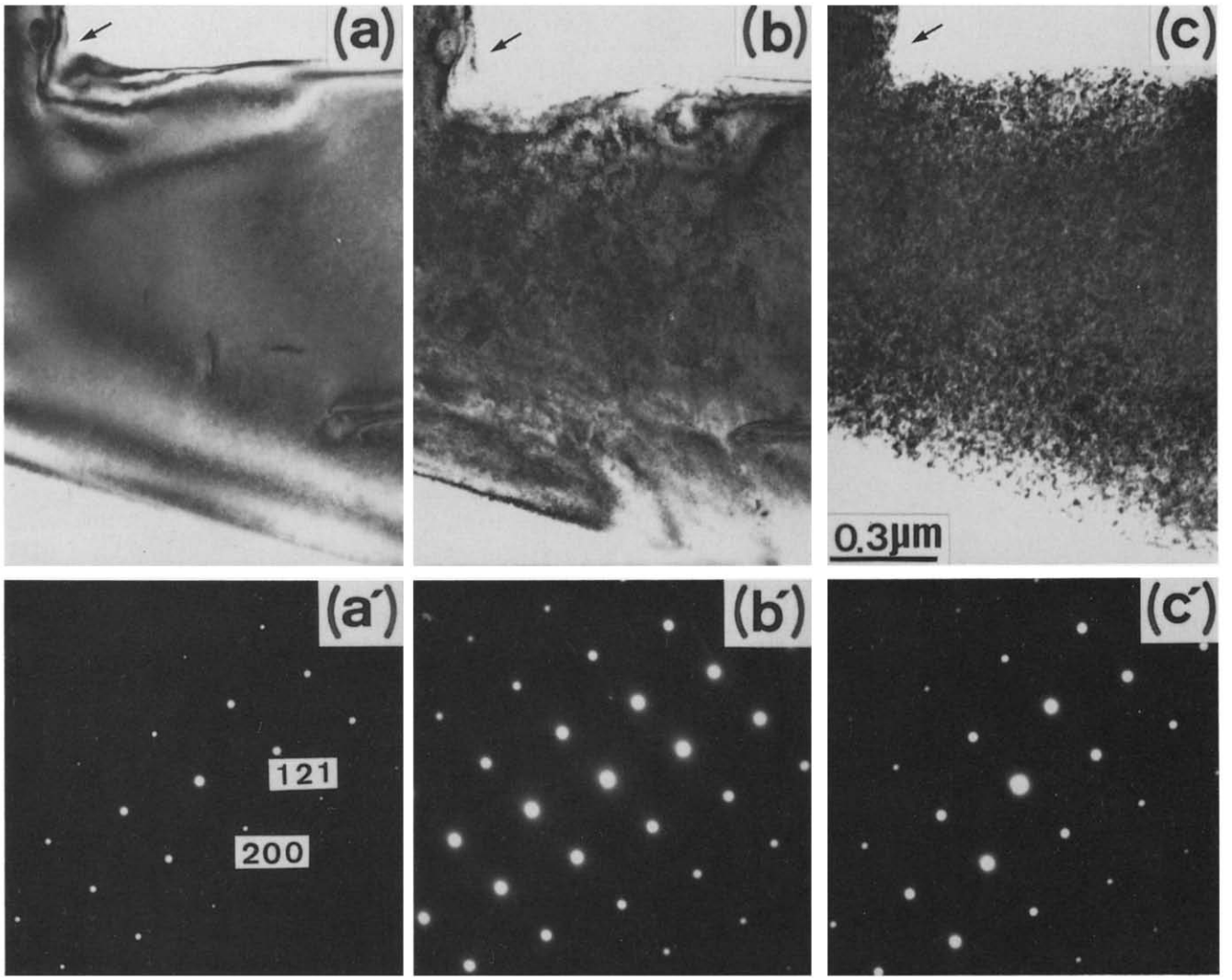

Fig. 2. *In-situ* irradiation sequence showing defect aggregation in Mn_2B. The arrows mark a fixed position. Irradiation temperature and flux were approximately 100 K and 1×10^{24} e m^{-2} s^{-1} respectively. (a) Before irradiation; (b) after irradiation for 360 s, (c) after irradiation for 3.6 ks. No signs of amorphization are recognized.

not in the electron-irradiation induced C–A transition of the transition metal borides. The criterion states that those compounds with narrow solubility ranges in the diagram tend to become amorphous under ion irradiation, whereas those with wide solubility ranges tend to remain crystalline. The present observation that TaB_2 with a wide solubility range of 8 at.% remains crystalline is not in contradiction with the criterion. However, all other 13 borides in Table 1 have almost no solubility, and eight out of the 13 become amorphous whereas the remaining five do not. It therefore seems reasonable to conclude that the solubility criterion is not applicable to the C–A transition by electron irradiation.

The form of the equilibrium phase diagram is known to provide a useful guide to the ease of amorphous material formation by liquid-phase quenching [12]. The amorphous forming ability of alloys is enhanced in the deep eutectic region of a phase diagram in the case of liquid-phase quenching. In the following, the observed amorphization tendency of transition metal borides under electron irradiation is discussed in terms of the position of the compounds in the corresponding phase diagram. In the nickel–boron binary system, there exist in total five equilibrium intermediate-phases, *i.e.* Ni_3B, Ni_2B, *o*-Ni_4B_3, *m*-Ni_4B_3 and NiB, as shown in Fig. 3. As seen from Table 1, of the five phases, Ni_2B and *o*-Ni_4B_3 can be rendered amorphous while Ni_3B, *m*-Ni_4B_3 and NiB remain crystalline under electron irradiation. The presence and absence of the C–A transition are shown in Fig. 3 by symbols ○ (amorphization) and × (no amorphization) respectively. Also given in the diagram is the composition range, LQ, over which amorphous materials can successfully be produced by the

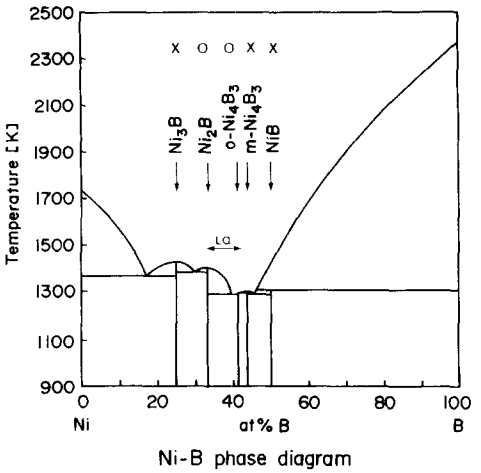

Fig. 3. Equilibrium phase diagram for the Ni–B system. The symbols ○ and × on the compounds represent presence and absence of the electron-irradiation induced amorphization in the compounds [8]. The composition range over which amorphous materials are successfully obtained by the liquid quenching technique [13] is marked as LQ.

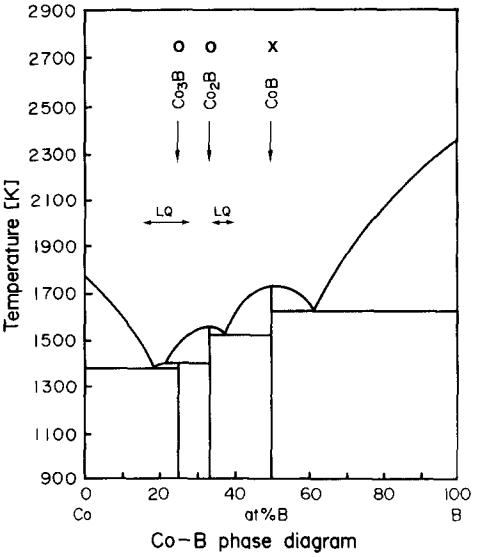

Fig. 4. Equilibrium phase diagram for the Co–B system. The symbols ○ and × on the compounds represent presence and absence of the electron-irradiation induced amorphization in the compounds [9]. The composition ranges over which amorphous materials are successfully obtained by the liquid quenching technique [13] are marked as LQ.

liquid quenching method [13]. It is evident from the diagram that Ni_2B and o-Ni_4B_3, which become amorphous, are located near the bottom of a deep valley of the liquid-phase region in the diagram and are situated within the composition range LQ, or immediately on the boundary of the composition range, whereas Ni_3B, m-Ni_4B_3 and NiB, which remain crystalline, are out of the range LQ. This fact suggests that the amorphization tendency under electron irradiation is similar to that obtained by the liquid quenching method in the nickel–boron system.

Another example of such a close correlation between the amorphization tendency and the position of the compounds in the phase diagram is found in the cobalt–boron binary system. In this system, there are three equilibrium intermediate-phases, *i.e.* Co_3B, Co_2B and CoB, as shown in Fig. 4. All these three borides were examined, and it was found that Co_3B and Co_2B can be rendered amorphous while CoB remains crystalline under electron irradiation, as shown in Table 1. These results are illustrated in the diagram in Fig. 4 by the symbols ○ (amorphization) and × (no amorphization). Also given in the diagram is the composition range, LQ, over which amorphous materials can successfully be produced by the liquid quenching method [13]. It is evident from the diagram that Co_3B and Co_2B, which become amorphous, are located near the bottom of a deep valley of the liquid-phase region and are situated within the composition range LQ, or immediately on the boundary of the composition range, whereas CoB, which remains crystalline, is out of the range LQ. A similar linkage between amorphization tendency under electron irradiation and the position of the compounds in the phase diagram is observed in all the alloy systems examined here; the results in the Mn–B, Fe–B and Ta–B systems are depicted in Figs. 5(a)–5(c) respectively (in these figures compounds without symbols ○ or × are those not examined in the present work).

From the above discussion it seems that the tendency toward the C–A transition under electron irradiation is best correlated with the position of the compounds in the temperature–composition phase diagram. Those compounds whose position in the phase diagram is close to the bottom of a deep valley of liquidus in the diagram have a strong tendency toward the C–A transition, while those removed from such a valley show little tendency toward the C–A transition. The reason why such parameters as the form of the phase diagram and the relative position of the compounds in the diagram are a good guide to the amorphization tendency, in contrast with the single parameters listed in Table 1, may be that the former parameters give more complete information as to the interaction among the constituent atoms.

To the present authors the fact that the compositions of liquid alloys which readily form amorphous solids upon quenching are quite similar to those of crystalline alloys (borides) which can readily be rendered amorphous by electron irradiation seems to be essential in considering the factor controlling the amorphization tendency of the alloys. As mentioned earlier, only the simplest types of lattice defects such as vacancies and interstitials are introduced into crystals under MeV electron irradiation, and quenching processes such as

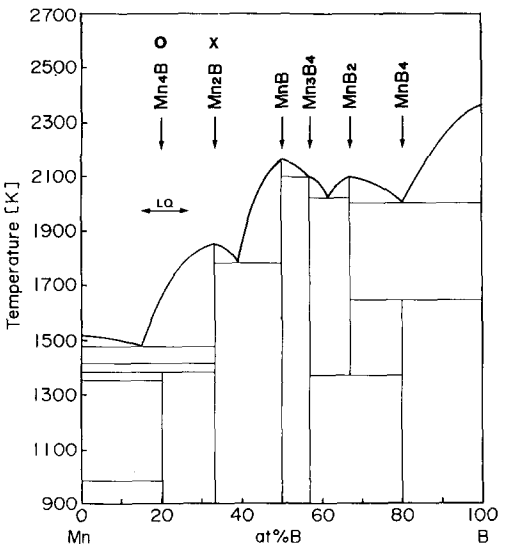

(a) Mn-B phase diagram

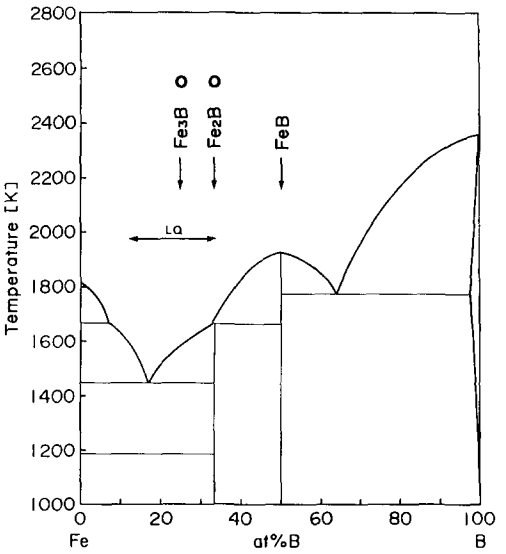

(b) Fe-B phase diagram

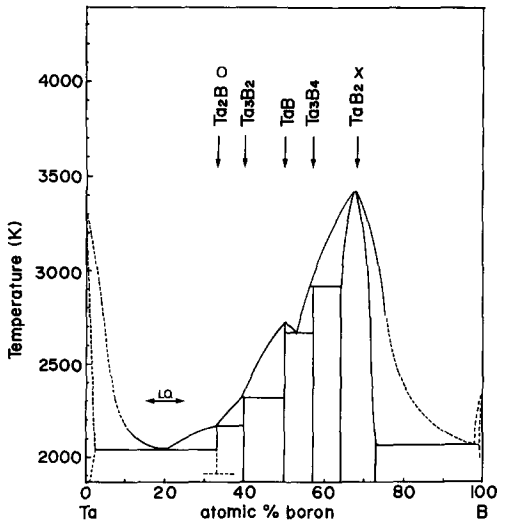

(c) Ta-B Phase Diagram

Fig. 5. Equilibrium phase diagrams for the systems: (a) Mn–B; (b) Fe–B; (c) Ta–B. The symbols ○ and × on the compounds represent presence and absence of the electron-irradiation induced amorphization in the compounds. The composition range over which amorphous materials are successfully obtained by the liquid quenching technique [14] is marked as LQ.

operate in the cascade core regions are absent. In other words, under electron irradiation crystals are rendered amorphous only through an accumulation of lattice defects and the interactions between them. From these considerations it follows that the mode of interaction among the lattice defects must be intrinsically different between crystals (borides) within the composition range where liquid alloys readily form amorphous solids upon quenching and those out of the composition range. The cause of the difference is directly correlated with the factor controlling the amorphization tendency. It is interesting to note here that the manifold in coordination, or in other words, the extent to which a variation is admissible in atomic coordination in the material, is suggested to be the most important parameter responsible for the difference [15].

References

1 G. Thomas, H. Mori, H. Fujita and R. Sinclair, *Scr. Metall., 16* (1982) 589–592.
2 H. Mori and H. Fujita, *Jpn. J. Appl. Phys., 21* (1982) L494–496.
3 A. Mogro-Campero, E. L. Hall, J. L. Walter and A. J. Ratkowski, in S. T. Picraux and W. J. Choyke (eds.), *Metastable Materials Formation by Ion Implantation*, North-Holland, Amsterdam, 1982, pp. 203–210.
4 G. J. C. Carpenter and E. M. Schulson, *J. Nucl. Mater., 23* (1978) 180–189.
5 H. Mori, M. Nakajima and H. Fujita, *Proc. 11th Inter. Congr. on Electron Microscopy, 1986*, The Japanese Society of Electron Microscopy, Tokyo, 1986, pp. 1101–1102.
6 H. Mori, H. Fujita, M. Tendo and M. Fujita, *Scr. Metall., 18* (1984) 783–788.

7 H. Mori and H. Fujita, *Proc. Int. Symp. Non-Equilibrium Solid Phases of Metals and Alloys*, Kyoto, Japan, *March 14–17, 1988*, Japan Inst. Metals, Sendai, 1988, pp. 93–96.
8 T. Sakata, H. Mori and H. Fujita, *J. Ceram. Soc. Jpn., 97* (1989) 289–294 (in Japanese).
9 T. Sakata, H. Mori and H. Fujita, *J. Ceram. Soc. Jpn., 97* (1989) 1379–1385 (in Japanese).
10 D. E. Luzzi and M. Meshii, *Scr. Met., 20* (1986) 943–948.
11 J. L. Brimhall, H. E. Kissinger and L. A. Charlot, *Radiat. Eff., 77* (1983) 273–293.
12 T. B. Massalski, in T. Masumoto and K. Suzuki, *Proc. 4th Int. Conf. on Rapidly Quenched Metals*, Japan Institute Metals, Sendai, 1981, pp. 203–208.
13 A. Inoue, A. Kitamura and T. Masumoto, *Trans. Jpn. Inst. Met., 20* (1979) 404–406.
14 U. Mizutani, Y. Hoshino and Y. Yamada, *A Manual for Amorphous Alloy Production*, AGNE, Tokyo, 1986.
15 H. Mori and H. Fujita, in A. R. Yavari (ed.), *Ordering and Disordering in Alloys*, Elsevier Applied Science, London and New York, 1992, pp. 277–286.